Optical absorption coefficient of quantum wires in strain and electric fields with intermixing interfaces

Johnson Lee
Department of Physics, Chung Yuan Christian University, Chung-Li, 32023 Taiwan

Harold N. Spector
Department of Physics, Illinois Institute of Technology, Chicago, Illinois 60616, USA

Wu Ching Chou
Department of Electrophysics, National Chiao Tung University, Hsin-Chu, 30010 Taiwan

Ying Sheng Huang
Department of Electronic Engineering, National Taiwan University of Science and Technology, Taipei, 10617 Taiwan
(Received 12 November 2004; revised manuscript received 28 June 2005; published 20 September 2005)

We have theoretically studied the optical absorption coefficient of quantum wires in electric and strain fields with intermixing interfaces. The potential profiles are governed by the intermixing heterojunctions, internal strain due to the lattice mismatch, the external electric field and stress. The second Fick's law describes the wires' intermixing heterojunctions due to the alloy interdiffusion. We adopt the Green's function method to solve the Poisson equation for the displacement to determine the internal strain due to the lattice mismatch. The single-band Schrödinger equation in the effective mass approximation is used to describe the conduction subband structures while the four-band Kohn-Luttinger Hamiltonian is used to describe the valence subband structures. In solving the Schrödinger equation and the Kohn-Luttinger Hamiltonian, we expand the wave functions for the electrons and holes by using linear combinations of the two-dimensional harmonic oscillator wave functions to yield two matrix equations. These matrix equations are numerically solved for their eigenenergies and their corresponding eigenfunctions. We investigate some physical properties of the unstrained quantum wire (GaAs/AlAs) and the strained wire (CdSe/ZnSe) as examples. When the interdiffusion becomes stronger, on one hand, the internal strain is relaxed leading to the band gap shrinkage (if the initial strain $\varepsilon_0 < 0$) and, on the other hand, the potential profiles are deformed and the effective band gap becomes wider. Variations of the transition energies with external stress show the anticrossing effect and variations of the transition energies with external electric field show the field emission effect. The hole effective masses can be enhanced or become electronlike by applying stress to the wire. The oscillator strengths of the dipole-allowed intersubband transitions for the y and z polarizations are calculated to infer possible optical transitions. The optical absorption coefficients together with the joint density of states are calculated.

DOI: 10.1103/PhysRevB.72.125329 PACS number(s): 78.67.Lt, 73.21.Hb, 73.63.Nm

I. INTRODUCTION

Advances in technology, especially using very accurate lithographic techniques, make it possible to confine electrons in quasi-one-dimensional semiconductor structures known as quantum wires[1,2] (QWR) with lateral widths down to 45 nm. Using recent developed crystal growth techniques on vicinal and patterned substrates,[3–5] QWR arrays with lateral dimensions less than 10 nm were fabricated. Among these arrays, the tilted superlattice[3] possesses rectangular cross sections and the serpentine superlattice[5] possesses parabolic lateral interfaces. The physics and applications of these semiconductor QWR structures have lead towards more flexible design[6] and improved device performance.[7,8] QWR lasers can be operated at lower threshold current densities[9,10] and increased gain and differential gain achieved by multidimensional confinement.[11] By using lattice-mismatched materials for the QWR lasers, the strain is expected to further enhance the gain.[11] However, when alloying or intermixing occurs during or after the growth process, the interfaces of the QWR become graded. A direct consequence of the graded-gap heterojunctions is a reduction of the strain due to the relaxation of the lattice mismatch. The atomic inter-diffusion can be achieved intentionally by using thermal annealing.[12]

In order to have a better understanding of the experimental results and to predict new physical properties of the QWR structures, more sophisticated theoretical modeling was developed to cope with all the new challenges. Unstrained QWR structures[13–18] such as GaAlAs/GaAs were investigated intensively and these results can serve as guidelines for more complex systems. Strained QWR structures[19–23] such as GaAlAs/GaInAs for long wavelength lasers are more difficult to study theoretically because the internal strain complicates the problems. Furthermore, electro-optical characterization of CdSe/ZnSe QD laser diodes has been reported,[24] and the lifetime of these devices has so far been limited to about 400 h in continuous wave operation.[25] Among these investigations, the most popular methods used to determine the subband structures is the Kohn-Luttinger Hamiltonian with four-band,[13,22] six-band,[15,23] or eight-band[19] models.

The energy profiles for the conduction and valence band edges can be distorted not only by the strain but also by the

atomic interdiffusion. The strain due to the lattice mismatch between the deposited material and the matrix material is a key feature of the quantum dots (QD) grown by the Stranski-Krastanov method.[26] For the self-assembled QD structures, the strain can cause large changes in both the band profiles and the carrier effective masses compared with their bulk values.[27] Therefore, similar deformations in the energy band profiles for the strained QWR structures are expected.[22] The strain distribution for QD structures with the anisotropy of the elastic properties can be calculated by means of the Green's function technique.[28] For the QWR structures, this same Green's function method can also be applied to investigate how the strain distribution deforms the energy band profiles. As crucial as the strain is the atomic interdiffusion which can make the abrupt interfaces become graded-gap heterojunctions and reduces the influence of the strain on the system. Such physical quantities as the Kohn-Luttinger parameters (or effective masses), deformation potentials, elastic constants, lattice constants, etc., must vary with the alloy composition. Therefore, the distribution of the alloy composition is crucial and can be calculated by solving the second Fick's law.[29] Experimental evidence of the interdiffusion for the CdSe/ZnSe QDs was reported.[30] Evidently, in order to calculate the energy subbands of nanostructures, we have to cope with not only the Kohn-Luttinger Hamiltonian but also with Fick's law for intermixing and the Poisson equation for the lattice displacement.

The main purpose of this paper is to investigate the optical absorption coefficient of the QWR with a rectangular cross section in strain and electric fields with intermixing interfaces. The distribution of the alloy composition of the QWR is calculated using the second Fick's law. There are two contributions to the strain. The internal contribution is due to the lattice mismatch while the external contribution is due to the applied stress. The internal strain is determined by solving the Poisson equation for the displacement with the Green's function method. We investigate how the external electric and stress fields, the internal strain and the atomic interdiffusion affect the potential profiles of the conduction and valence band edges, the subband structures, joint density of states, oscillator strengths, and optical absorption coefficient. In Sec. II, a theoretical model is presented to describe how the above affect the energy band edges, the energy subband structures, and other physical properties of the system. Section III presents our numerical results and detailed discussions. We study some optical properties of the unstrained GaAs/AlAs and strained CdSe/ZnSe QWRs. Finally, our conclusions are presented in Sec. IV.

II. THEORETICAL MODEL

Consider a rectangular QWR with dimensions of a along the y axis and b along the z axis. Choose the z direction to be the crystal growth direction [001] and let the x axis pass through the center of the rectangular cross section of the wire. Quasiparticles are confined in the y and z directions while they can propagate freely in the x direction. The QWR is buried in a matrix material. Let the material of the QWR be a binary compound AD (A=Ga, D=As or A=Cd, D=Se), with a smaller energy gap E_{gw} while the material of the matrix is a different binary compound BD (B=Al or B=Zn), with a larger energy gap E_{gm}. The band gap difference is $\Delta E_g = E_{gm} - E_{gw}$ while the conduction band offset is Q_c. An electric field F_y in the y direction and a stress Z_z in the z direction are applied to the QWR. We consider three contributions to the energy shifts for the conduction band edge $E_c(y,z)$ and the valence band edge $E_v(y,z)$: (i) the interdiffusion, (ii) the internal strain ε_{ij} and the external stresss Z_z, and (iii) the external electric field F_y. A description of these three contributions follows.

A. Intermixing interfaces

Assume that the atomic interdiffusion can occur and atoms A and B can exchange. The material near the interfaces of the QWR and the matrix becomes ternary, $A_cB_{1-c}D$, where c is the composition of the atom A in the wire. The second Fick's law governs the evolution of the composition $c(y,z,t)$ and is given by

$$\frac{\partial c}{\partial t} = \left(D_y \frac{\partial^2}{\partial y^2} + D_z \frac{\partial^2}{\partial z^2} \right) c, \tag{1}$$

where D_y, D_z are the interdiffusion coefficients which depend upon the directions and the temperature of the system. The general solution of Eq. (1) for a cross section of an arbitrary shape is derived as

$$\begin{aligned} c(y,z,t) = \frac{1}{(2\pi)^2} \iint_{\Omega} dy'\, dz' \chi(y',z') \iint_{Q} dq_y\, dq_z \\ \times \exp i[q_y(y-y') + q_z(z-z')] \\ \times \exp[-t(D_y q_y^2 + D_z q_z^2)], \end{aligned} \tag{2}$$

where $\chi(y,z)$ is the characteristic function of the QWR, which is equal to unity within the QWR and zero outside, Ω is the volume of the entire system (QWR plus matrix), and Q spans the entire Fourier space for the Fourier components q_y and q_z. At room temperature the diffusion coefficients D_y and D_z are small but when one anneals the system at high temperatures D_y and D_z increase and interdiffusions also are greatly enhanced. The annealing time is $t=\tau$. After the annealing stops, the interdiffusion process becomes negligible. We define the diffusion parameters $L_y=(D_y\tau)^{1/2}$ and $L_z=(D_z\tau)^{1/2}$ which are the characteristic diffusion lengths. For the case of a QWR with a rectangular cross section with dimensions a and b, the composition c of the ternary compound $A_cB_{1-c}D$ is

$$\begin{aligned} c(y,z,\tau) &= F_{\mathrm{Dy}}(y) F_{\mathrm{Dz}}(z), \\ F_{\mathrm{Dy}}(y) &= \frac{1}{2}\left[\mathrm{erf}\left(\frac{a/2-y}{2L_y} \right) + \mathrm{erf}\left(\frac{a/2+y}{2L_y} \right) \right], \\ F_{\mathrm{Dz}}(z) &= \frac{1}{2}\left[\mathrm{erf}\left(\frac{b/2-z}{2L_z} \right) + \mathrm{erf}\left(\frac{b/2+z}{2L_z} \right) \right], \end{aligned} \tag{3}$$

where $\mathrm{erf}(x)$ is the error function. The contribution of the interdiffusion to the energy shift for the conduction (valence) band edge is $\Delta E_c^{\,d}$ ($\Delta E_v^{\,d}$) and is given by

$$\Delta E_c^{\,d}(y,z) = Q_c \Delta E_g[1 - c(y,z,\tau)],$$

$$\Delta E_v^{\,d}(y,z) = (1 - Q_c)\Delta E_g[1 - c(y,z,\tau)], \tag{4}$$

where the superscript d indicates the diffusion. Equation (4) implies that if the interdiffusion is weak, i.e., L_y and $L_z \approx 0$, the composition $c(y,z,\tau)$ for the atom A (in the QWR) becomes the characteristic function $\chi(y,z)$ of the QWR. Thus, the interface is abrupt as expected. When L_y and L_z are large a lot of A atoms move out from the QWR to the matrix and $\Delta E_c^{\,d}$ and $\Delta E_v^{\,d}$ are reduced. Thus, the interface becomes graded. Here, $\Delta E_c^{\,d}$ and $\Delta E_v^{\,d}$ determine the energy profiles of the intermixing interfaces due to the interdiffusion.

B. Strain distribution

Since the QWR experiences the strains from two different causes, we discuss them separately.

1. Internal strain

The lattice constant for the QWR material is a_w and for the matrix is a_m. For cubic crystals, the initial strain is $\varepsilon_0 = (a_m - a_w)/a_w$. The strain distribution is calculated by means of the Green's function method[28] for solving the Poisson equation for the displacement. The original purpose of Ref. 28 was to calculate the strain distribution in QDs of arbitrary shape. We follow the same line and apply their result to the QWR case. The Fourier transform of the strain tensor ε_{ij} for QWR with cubic symmetry is[27,28]

$$\bar{\varepsilon}_{ij}(\vec{\xi}) = \varepsilon_0 \bar{c}(\vec{\xi}) \left\{ \delta_{ij} - \frac{(C_{11} + 2C_{12})\xi_i \xi_{i'}/\xi^2}{1 + (C_{12} + C_{44}) \sum_{k=1}^{3} \dfrac{\xi_k^2}{C_{44}\xi^2 + C_{\mathrm{an}}\xi_k^2}} \times \frac{1}{2}\left[\frac{1}{C_{44} + C_{\mathrm{an}}\xi_i^2/\xi^2} + \frac{1}{C_{44} + C_{\mathrm{an}}\xi_j^2/\xi^2} \right] \right\}, \tag{5}$$

where C_{11}, C_{12}, and C_{44} are the elastic moduli, $C_{\mathrm{an}} = C_{11} - C_{12} - 2C_{44}$ describes the anisotropic part of the tensor, $\xi_x = 0$ and $\xi = (\xi_y^{\,2} + \xi_z^{\,2})^{1/2}$ with $k = 1$, 2, and 3 represent x, y, and z, respectively. The QWR shape enters in Eq. (5) only in the form of the Fourier transform of $c(y,z,\tau)$ which is defined in Eq. (3). The quantities ξ_i in Eq. (5) are components of ξ. We have

$$\bar{c}(\vec{\xi}) = \int_{-\infty}^{\infty} dy \exp(i\xi_y y) F_{\mathrm{Dy}}(y) \int_{-\infty}^{\infty} dz \exp(i\xi_z z) F_{\mathrm{Dz}}(z). \tag{6}$$

The strain tensor ε_{ij} can be obtained by performing the inverse Fourier transform of Eq. (5). Although GaAs has the cubic structure, CdSe can have the cubic and wurtzite structures. The primitive translation vectors for the wurtzite structure are listed in Ref. 31. The zinc blende phase CdSe grown on cubic GaAs by the molecular beam epitaxy was reported.[32] By appropriately choosing weighting factors for ξ_i in Eq. (5), the result is applicable for the wurtzite structure. The effective mass Hamiltonian for the wurtzite compounds can be found in Ref. 32. In this paper, we investigate only the cubic case. The strain Hamiltonian takes the same form as the effective mass Hamiltonian.

The strain Hamiltonian[33] H_ε in a spin 3/2 basis: $[u_{-3/2}, u_{-1/2}, u_{1/2}, u_{3/2}]$ for a valence band without spin-orbital interaction is

$$H_\varepsilon = \begin{bmatrix} -p+q & -s^* & r & 0 \\ -s & -p-q & 0 & r \\ r^* & 0 & -p-q & s^* \\ 0 & r^* & s & -p+q \end{bmatrix} \tag{7}$$

with

$$p = a_v(\varepsilon_{xx} + \varepsilon_{yy} + \varepsilon_{zz}) = a_v \varepsilon_{hy},$$

$$q = b_v\left(\varepsilon_{zz} - \frac{1}{2}(\varepsilon_{xx} + \varepsilon_{yy}) \right) = b_v \varepsilon_{\mathrm{sh}},$$

$$r = \frac{\sqrt{3}}{2} b_v(\varepsilon_{xx} - \varepsilon_{yy}) - i d_v \varepsilon_{xy},$$

$$s = -d_v(\varepsilon_{xz} - i\varepsilon_{yz}), \tag{8}$$

where ε_{ij} is determined by the inverse Fourier transform of Eq. (5), a_v is the hydrostatic valence band deformation potential, b_v and d_v are the shear deformation potentials, $\varepsilon_{\mathrm{hy}}$ is the hydrostatic strain, and $\varepsilon_{\mathrm{sh}}$ is the shear strain. The energy shifts for the valence band edge due to the internal strain are $-\Delta E_v^{\,\varepsilon}$ and can be obtained by solving the eigenvalue problem of Eq. (7). We obtain

$$\Delta E_{v\pm}^{\varepsilon} = a_v \varepsilon_{hy} \pm \sqrt{\tfrac{3}{4} b_v^{\,2}(\varepsilon_{xx} - \varepsilon_{yy})^2 + (d_v \varepsilon_{yz})^2 + (b_v \varepsilon_{\mathrm{sh}})^2}. \tag{9}$$

Here we see that the twofold degeneracy of the valence band edge is removed because of the strain due to the lattice mismatch. The strain Hamiltonian for the conduction band edge is assumed to be in a spin 1/2 basis. The energy shift for the conduction band edge due to the internal strain is $\Delta E_c^{\,\varepsilon}$ and is given by

$$\Delta E_c^{\,\varepsilon} = a_c \varepsilon_{hy}, \tag{10}$$

where a_c is the hydrostatic conduction band deformation potential. The total energy shift ΔE^{ε} due to the internal strain is $\Delta E_c^{\,\varepsilon} - \Delta E_{v\pm}^{\,\varepsilon}$. Note that in this paper, the total deformation potential energy a_{tot} is defined as $a_c - a_v$ and this relationship is used in Table I.

2. External stress

Assume that a stress Z_z in the z direction is applied to the QWR. By solving Hooke's law for the strain components and the stress components, we obtain $\varepsilon_{xx} = \varepsilon_{yy} = S_{12} Z_z$, $\varepsilon_{zz} = S_{11} Z_z$, and $\varepsilon_{ij} = 0$ if $i \neq j$, where S_{ij} is the compliance constant. Let H_z be the external stress Hamiltonian which has the same mathematical form as H_ε defined in Eq. (7) with a new set of p, q, r, s: $p = a_v(S_{11} + 2S_{12})Z_z$, $q = b_v(S_{11} - S_{12})Z_z$, $r = 0$, $s = 0$. Because the components r and s are zero, the stress

TABLE I. Input material parameters used in the calculations.

	GaAs	Ref.	AlAs	Ref.	CdSe	Ref.	ZnSe	Ref.
E_g (eV)	1.428	19	2.447	19	1.765	40	2.821	40
a (nm)	0.56533	19	0.56605	19	0.6077	41	0.56676	41
m_e^*/m_e	0.067	19	0.15	19	0.13	41	0.16	41
γ_1	7.1	19	3.76	19	2.04	42	3.77	43
γ_2	2.02	19	0.9	19	0.58	42	1.24	43
γ_3	2.91	19	1.42	19	0.58	42	1.67	43
a_c (eV)	−8.013	19	−5.64	19	−2.336	40[a]	−2.71	40 and 44
a_v (eV)	2.20	19	2.47	19	1.328	40[a]	1.54	32 and 39
b_v (eV)	−1.824	19	−1.7	19	−0.8	40	−1.2	40
d_v (eV)	−5.062	19	−4.55	19	−2.9	45	−5.4	45
C_{11} (Gpa)	118.8	19	120.2	19	74.2	46	88.8	46
C_{12} (Gpa)	53.8	19	57	19	45.3	46	52.7	46
C_{44} (Gpa)	59.4	19	58.9	19	13.4	46	44.1	46
κ	13.1	39	10.1	39	10.6	47	8.1	47
Δ (eV)	0.34	19	0.28	19	0.42	48	0.43	48

[a] a_c and a_v for CdSe are not known. We assume that the ratio of a_c/a_v for CdSe is same as the ratio for ZnSe.

Hamiltonian H_z is diagonalized. The energy shifts $\Delta E_c{}^Z$ and $\Delta E_{v\pm}{}^Z$ due to the external stress Z_z for the conduction and valence band edges are

$$\Delta E_c^Z = \left(\frac{a_c}{C_{11}+2C_{12}}\right) Z_z,$$

$$\Delta E_{v\pm}^Z = \left(\frac{a_v}{C_{11}+2C_{12}} \pm \frac{b_v}{C_{11}-C_{12}}\right) Z_z \tag{11}$$

and the total energy shift ΔE^Z due to Z_z is $\Delta E_c{}^Z - \Delta E_v{}^Z$. Similar to the internal strain, Z_z can remove the degeneracy of the valence band edge and split the band edge.

C. Applied electric field

Consider that an electric field F_y in the y direction is applied to the QWR of dimension a. For simplicity, we assume that F_y is a constant field by ignoring the spatial variation of the dielectric constant. If there is not too great a difference between the dielectric constants in the wire and in the barrier, this is a good approximation. Let $\Delta E_c{}^F(\Delta E_v{}^F)$ be the energy shift due to the electric field F_y for the conduction (valence) band edge. We take $\Delta E_c{}^F$ and $\Delta E_v{}^F$ to be zero at $y=-a/2$ as the boundary condition. The energy shift due to F_y is a linear function of y:

$$\Delta E^F = \Delta E_c{}^F = \Delta E_v{}^F = eF_y(y+a/2), \tag{12}$$

where e is the electron charge. When an electric field is applied to the QWR, both the conduction and valence band edges become tilted.

D. Energy band edge

Under the flat band conditions, all internal and external fields are ignored, i.e., F_y, Z_z, ε_0 and L_y and L_z are zero. We take the zero-energy point at the center of the wire ($y=0$, $z=0$). The conduction and valence band edges as a function of position (y,z) are given by

$$E_c(y,z) = Q_c \Delta E_g[1-\chi(y,z)],$$

$$E_v(y,z) = -E_{gw} - (1-Q_c)\Delta E_g[1-\chi(y,z)]. \tag{13}$$

When external and internal fields are turned on, the energy bands are no longer flat and are described by

$$E_c(y,z) = \Delta E_c{}^d + \Delta E_c{}^\varepsilon + \Delta E_c{}^Z + \Delta E_c{}^F,$$

$$E_{v\pm}(y,z) = -E_{gw} - \Delta E_v{}^d - \Delta E_{v\pm}{}^\varepsilon - \Delta E_{v\pm}{}^Z - \Delta E_v{}^F. \tag{14}$$

When all fields are turned off, Eq. (14) reduces to Eq. (13). We define $E_c - E_{v\pm}$ as the effective energy band gaps. For the GaAs/AlAs (CdSe/ZnSe) system, the effective band gap increases as the Ga (Cd) concentration $c(y,z,\tau)$ in the QWR decreases and the Al (Zn) concentration $1\text{-}c(y,z,\tau)$ increases. A discussion of the energy subband structures of the quasiparticles with the potential profiles E_c and E_v is to follow.

E. Energy subband structures

To calculate energy subbands for the electrons and holes, we assume that for simplicity, the conduction and valence band are decoupled as proposed by Cusack *et al.*[34] The general solution for the electron in the jth state in a spin 1/2 basis is

$$\Psi_j^c(x,y,z) = \frac{\exp(ik_x x)}{\sqrt{2\pi}} u^c \Phi_j^c(y,z), \tag{15}$$

where k_x is the wave vector, u^c is a bulk conduction band edge Bloch function, $\Phi_j{}^c$ is the jth envelope function in the effective mass approximation satisfying the single-band Schrödinger equation

$$-\left(\nabla\frac{\hbar^2}{2m_e^*(y,z)}\cdot\nabla\right)\Phi^c(y,z)+\left[V_c(y,z)+\frac{\hbar^2k_x^2}{2m_e^*(y,z)}\right]\Phi^c(y,z)=E^c\Phi^c(y,z). \quad (16)$$

Here E^c and Φ^c are the eigenenergy and the eigenfunction, respectively, and m_e^* is the electron effective mass, $V_c=E_c(y,z)$ is the confinement potential energy for the electrons and is defined in Eq. (14).

The valence band states are calculated by using the four-band Kohn-Luttinger Hamiltonian H_h in a spin 3/2 basis[33] $[u_{-3/2},u_{-1/2},u_{1/2},u_{3/2}]$ has the same form as H_ε in Eq. (7)

$$H_h=\begin{bmatrix} -P+Q & -S^* & R & 0\\ -S & -P-Q & 0 & R\\ R^* & 0 & -P-Q & S^*\\ 0 & R^* & S & -P+Q\end{bmatrix} \quad (17)$$

with

$$-P+Q=E_{gw}+\frac{\hbar^2}{2m_e}[-(\gamma_1-\gamma_2)k_x^2+\partial_y(\gamma_1-\gamma_2)\partial_y+\partial_z(\gamma_1+2\gamma_2)\partial_z],$$

$$-P-Q=E_{gw}+\frac{\hbar^2}{2m_e}[-(\gamma_1+\gamma_2)k_x^2+\partial_y(\gamma_1+\gamma_2)\partial_y+\partial_z(\gamma_1-2\gamma_2)\partial_z],$$

$$R=\sqrt{3}\frac{\hbar^2}{2m_e}[-\gamma_2k_x^2-\partial_y\gamma_2\partial_y+k_x(\gamma_3\partial_y+\partial_y\gamma_3)],$$

$$S=i\sqrt{3}\frac{\hbar^2}{2m_e}[\partial_z\gamma_3\partial_y+\partial_y\gamma_3\partial_z-k_x(\gamma_3\partial_z+\partial_z\gamma_3)], \quad (18)$$

where m_e is the free electron mass, $\gamma_1,\gamma_2,\gamma_3$ are the Kohn-Luttinger parameters, and k_x is the wave vector in the x direction. Note that the original H_h is not Hermitian and a symmetrized procedure[19] is performed to yield Eq. (18). We note that by using this symmetrized Hamitonian, some of the intrinsic properties of the heterointerface are completely ignored.[35–37] The energy sub-bands for holes are calculated using the Schrödinger equation

$$[H_h+H_\varepsilon+H_z-V_h(y,z)]\Phi^v(y,z)=E^h\Phi^v(y,z),\quad v=1,2,3,4, \quad (19)$$

where H_ε is for the internal strain, H_z is for the external stress Z_z, and V_h is the confinement potential for holes and is governed by $\Delta E_v^{\,d}$ due to the interdiffusion and $\Delta E_v^{\,F}$ due to the electric field F_y. The valence band wave function for the ith state is given by

$$\Psi_i^h(x,y,z)=\frac{\exp(ik_xx)}{\sqrt{2\pi}}\sum_{v=1}^{4}u^v\Phi_i^v(y,z), \quad (20)$$

where u^v is a bulk valence band edge Bloch function in a spin=3/2 basis.

In order to solve the Schrödinger equation given by Eq. (16) for electrons and Eq. (20) for holes, we expand Φ^c and Φ^v into a linear combination of a set of orthonormal basis functions. We adopt the two-dimensional harmonic oscillator wave functions as the basis and write

$$\Phi^c(y,z)=\sum_{mn}A_{mn}Y_m(y)Z_n(z),$$

$$\Phi^v(y,z)=\sum_{mn}B_{mn}^vY_m(y)Z_n(z)\quad(v=1,2,3,4),$$

$$Y_m(y)=(\sqrt{\pi}2^m m!y_0)^{-1/2}\exp(-q_y^2/2)H_m(q_y),$$

$$Z_n(z)=(\sqrt{\pi}2^n n!z_0)^{-1/2}\exp(-q_z^2/2)H_n(q_z), \quad (21)$$

where H_n is the nth Hermite polynominal, A_{mn} and $B_{mn}^{\,v}$ are the appropriate expansion coefficients to be determined. We define $q_y=y/y_0$ and $q_z=z/z_0$ with the respective classical turning points y_0 in the y direction and z_0 in the z direction. Here we see that when y and z approach infinity, Φ^c and Φ^v automatically go to zero. Because of the interdiffusion, there are many position dependent parameters: $m_e^*,\gamma_1,\gamma_2,\gamma_3,a_c,a_v,b_v,d_v,\ldots$, and we assume that these parameters vary linearly with the composition $c(y,z,\tau)$. By substituting Φ^c and Φ^v in Eq. (21) into Eq. (16) for the electrons and Eq. (19) for the holes, respectively, we multiply Eqs. (16) and (19) by Y_m,Z_n, and then integrate over the entire volume of the system to yield matrix equations for the electrons and holes, respectively. After solving the matrix equations, the expansion coefficients A_{mn} and $B^v{}_{mn}$, together with the eigenenergies $E^c{}_i(k_x)$ for the conduction subband structures and $E^h{}_j(k_x)$ for the valence subband structures with i and $j=1,2,3,\ldots$, are determined.

F. Some physical properties

In the QWR, quasiparticles are confined laterally and allowed to move freely in the x direction. The joint density of states plays important role in laser applications and is defined as

$$J_{cv}=\frac{1}{2\pi}\sum_{j=1}^{J}\sum_{i=1}^{I}\int_K dk_x\,\delta[E_j^c(k_x)-E_j^h(k_x)-\hbar\omega], \quad (22)$$

where $I(J)$ is the maximum number of subbands for holes (electrons) in the QWR and $\hbar\omega$ is the optical photon energy. The optoelectronic properties of the QWR structures can be formulated from first order perturbation theory. The optical absorption coefficient for polarization in the $\hat{e}$ direction in c.g.s. is given by[31]

$$\alpha=\frac{4\pi e^2\hbar}{m_e^2c_0n_0ab}\sum_{ij}\int_{-\infty}^{\infty}dk_x\frac{|\langle\Psi_j^c|e\cdot p|\Psi_i^h\rangle|^2}{[E_j^c(k_x)-E_i^h(k_x)]}\delta[E_j^c(k_x)-E_i^h(k_x)-\hbar\omega], \quad (23)$$

where $\psi^c{}_j$ [Eq. (15)] and $\psi^h{}_i$ [Eq. (20)] are the wave functions for the electron in the jth subband and for the hole in the ith subband, respectively, ab is the area of the wire's cross section, n_0 is the index of refraction, c_0 is the speed of light, $\hbar\omega$ is the photon energy. Substituting Eqs. (15) and

(20) into Eq. (23) with the help of the orthnormal property of the harmonic oscillator wave functions, the expression of Eq. (23) is simplified to

$$\alpha = \frac{2\pi e^2\hbar}{m_e c_0 n_0 ab}\int_K dk_x \sum_{ij} O_{ji}(k_x)\,\delta[E_j^c(k_x) - E_i^h(k_x) - \hbar\omega]$$

$$Q_{ji}(k_x) = \frac{\sum_{v=1}^{4} g^v(\hat{e})\left|\sum_{mn} A_{mn}(k_x)B_{mn}^v(k_x)\right|^2}{E_j^c(k_x) - E_i^h(k_x)}\left(\frac{2P_{cv}^2}{m_e}\right), \quad (24)$$

where $g^1(\hat{e})=g^4(\hat{e})=1/2$, $g^2(\hat{e})=g^3(\hat{e})=1/6$ for the polarization $\hat{e}$ in the y direction and $g^1(\hat{e})=g^4(\hat{e})=0$, $g^2(\hat{e})=g^3(\hat{e})=2/3$ for the polarization $\hat{e}$ in the z direction, $O_{ji}(k_x)$ is the oscillator strength which represents the equivalent number of oscillators for the transition between the valence and conduction subbands, P_{cv} (Ref. 38) is a constant. For numerical purposes, we replace the delta function by the Lorenzian

$$\delta(x) \to \frac{1}{\pi}\left(\frac{\Gamma}{x^2+\Gamma^2}\right), \quad (25)$$

where Γ is the half width at half maximum (HWHM). For convenience in our later discussion, we set the difference between $E_j^c(k_x)$ and $E_i^h(k_x)$ to

$$\Delta E_{ji}(k_x) = E_j^c(k_x) - E_j^h(k_x) \quad (26)$$

and we call $\Delta E_{ji}(k_x=0)$ the optical transition energy.

III. NUMERICAL RESULT AND DISCUSSION

We investigate some physical properties of the strained and unstrained QWRs with intermixing interfaces. The dimensions of the wire's cross section under study is $a=10$ nm along the y axis (width) and $b=2$ nm along the z axis (thickness) which give an aspect ratio of $a:b=5:1$. Table I lists the parameters for the numerical calculations. The lattice constants a listed in Table I show that the initial strain ε_0 for GaAs/AlAs QWR is 0.1274% (nearly perfect lattice match) and for CdSe/ZnSe QWR is −6.7369%. Thus, for the unstrained case due to the lattice match, we use the GaAs/AlAs QWR as a numerical example while for the strained case due to the lattice mismatch, we use the CdSe/ZnSe QWR as a numerical example. We take the conduction band offset Q_c for the GaAs/AlAs (Ref. 39) QWR to be 0.3 and for the CdSe/ZnSe (Ref. 40) QWR to be 0.78 for our numerical calculations. For numerical convergence purpose, appropriate choices of the classical turning points y_0 and z_0 are vital. For a rectangular cross section, it is natural to choose $y_0=\pm a/2$ and $z_0=\pm b/2$ to have good convergence. We investigate the influences of the interdiffusion parameters $L_y=L_z=L$, internal strain ε_0, external stress Z_z, and electric field F_y on the physical properties of unstrained and strained QWRs. Discussions of our results are in the following.

A. Unstrained GaAs/AlAs QWR

The energy band profiles of Eq. (14) for the GaAs/AlAs QWR as a function of y is plotted in Fig. 1 with following parameters: the diffusion parameter $L_y=L_z=L=1$ nm, $F_y=6$ mV/nm, $Z_z=-4$ GPa (compression) at $z=0$. Figure 1 shows that under the flat band conditions ($L_y=L_z=L=0$, $F_y=0$, $Z_z=0$, $\varepsilon_0=0$), the energy profiles are step functions (abrupt interfaces). When all the fields are turned on ($L_y=L_z=L=1$ nm, $F_y=6$ mV/nm, $Z_z=-4$ GPa, $\varepsilon_0=0.1274\%$), (i) the external compression causes the valence band edge to split into two branches and widens the effective band gap (i.e., $E_c-E_{v\pm}>E_{gw}$), (ii) the internal strain makes no significant contribution to the band edge shifts because ε_0 is too small (nearly lattice matched), (iii) the interdiffusion makes the sharp heterojunctions become gradual, and (iv) the electric field F_y tilts both the conduction and valence band edges. Note that since the external compression is applied to the entire system, the compression splits both the valence band edges of the wire and matrix materials as shown in Fig. 1. When the QWR is stress free ($Z_z=0$) and there is no electric field ($F_y=0$), the valence and conduction subband energies at the zone center and the optical transition energy ΔE_{ji} (0) as a function of the diffusion parameters $L_y=L_z=L$ are plotted in Figs. 2(a)–2(c), respectively. When L increases, more Al atoms (Ga atoms) diffuse into (out of) the wire and the effective band gap of the wire becomes larger. This can be seen from Eq. (4) where when the concentration of Ga atoms in the wire decreases, the electron energy increases and the hole energy decreases thereby increasing the band gap. Figure 2(a) shows that the lowest six valence subband energies $E^h{}_j(0)$ ($j=1-6$), decrease (become more negative) as the diffusion parameter L increases. Figure 2(b) shows that the lowest two conduction subband energies $E^c{}_j(0)$ ($j=1,2$) increase almost linearly as L increases. The transition energies $\Delta E_{ji}(0)$ increase as L increases as depicted in Fig. 2(c). This implies that when an electron and a hole recombine, the emitted light shows blueshifts as the diffusion parameter increases. In our model, the sub-band

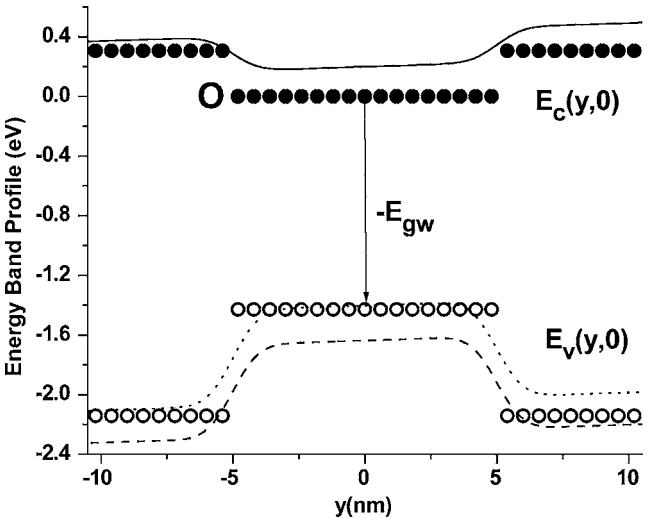

FIG. 1. Energy band profile for the GaAs/AlAs QWR structure. For the flat bands, ● represents the conduction band edge; ○ represents the valence band edge. When the external fields, F_y and Z_z are applied to the QWR, the solid curve is for E_c, the dotted curve is for E_{v+}, and the dashed curve is for E_{v-}. O is the energy reference point.

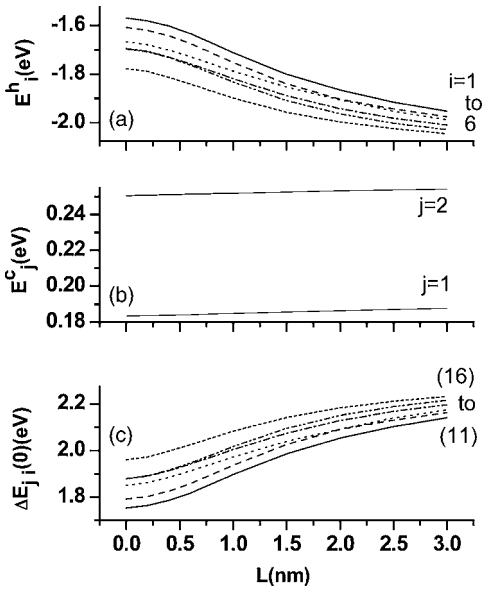

FIG. 2. (a) Valence subbands E^h_i, (b) conduction subbands E^c_j, and (c) ΔE_{ji} at zone center as a function of the diffusion parameter $L_{y,z}=L$ without any external fields for the GaAs/AlAs QWR.

structures for the conduction electrons obtained from Eq. (16) are nearly parabolic because the spatial variation of the effective mass is small. The lowest six valence subband structures $[E^h_i(k_x), i=1-6]$ for the QWR with $L=1$ nm, $Z_z=0$, $F_y=0$ and with $L=1$ nm, $Z_z=-4$ Gpa, $F_y=0$ are plotted in Figs. 3(a) and 3(b), respectively. At the zone center, in Fig. 3(a), $E^h_i(0)$ in eV are $-1.712\{-\}$, $-1.752\{+\}$, $-1.787\{-\}$, $-1.819\{+\}$, $-1.832\{-\}$, and $-1.898\{+\}$; and in Fig. 3(b), $E^h_i(0)$ in eV are $-1.664\{-\}$, $-1.690\{-\}$, $-1.755\{+\}$, $-1.808\{-\}$, $-1.842\{-\}$, and $-1.909\{+\}$. The curvatures of $E^h_i(0)$ are marked with $\{+\}$ for upward curvature and $\{-\}$ for downward curvature. By examining the probability densities $|\Phi^v|^2$ with $v=1,2,3,4$,

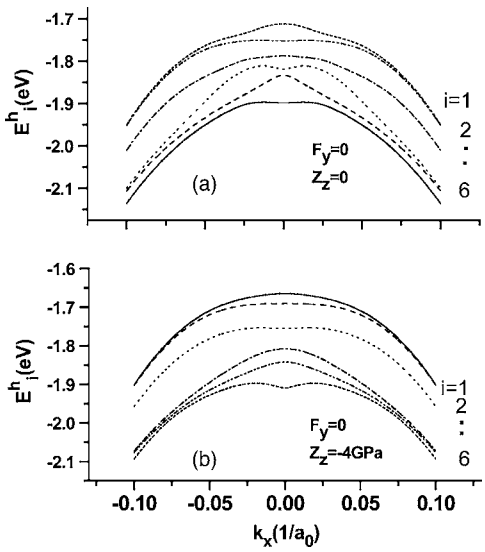

FIG. 3. Valence subband structures for (a) without external fields, and (b) with a stress for the GaAs/AlAs QWR.

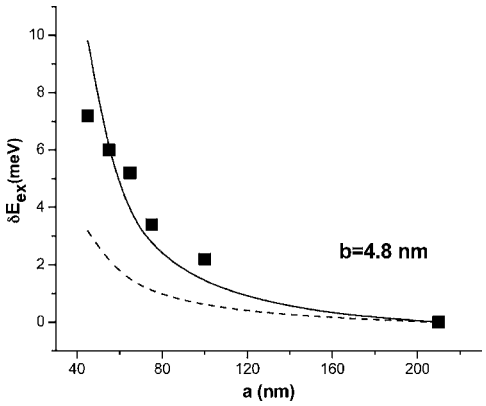

FIG. 4. The observed dependence of the blueshift in the photoluminescence on wire width of a is marked with ■ for a fixed wire thickness of $b=4.8$ nm. Theoretical predications are plotted with the solid curve for different diffusion parameters $L_y=8$ nm and $L_z=0.2$ nm. For comparison the dashed curve is plotted without diffusion. [2 K parameters: $E_{gw}=1.519$ eV, $E_{gb}=3.099$ eV (Ref. 49) $Q_c=0.57$ (Ref. 50)].

in Eq. (21), we find that the corresponding eigenfunctions of the eigenenergy $E^h_i(k_x)$ are a mixture of the spin 3/2 basis: $[u_{-3/2}, u_{-1/2}, u_{1/2}, u_{3/2}]$. At the zone center with $Z_z=0(-4$ GPa), we have probability densities $|\Phi^1|^2=0.013(0.8274)$, $|\Phi^2|^2=0.0351(0.0123)$, $|\Phi^3|^2=0.9392(0.0063)$, and $|\Phi^4|^2=0.0127(0.1539)$. Thus the $u_{1/2}(u_{-3/2})$ is the dominant component, and we call that state light- (heavy-) hole-like. With decreasing $GaAs/Al_{0.33}Ga_{0.67}As$ wire width of a an increasing blueshift of the wire luminescence energy at 2 K due to rapid thermal anneal was observed[1] and plotted in Fig. 4 for a fixed wire thickness of $b=4.8$ nm. The energy shift of the ground state heavy-hole exciton $\delta E_{ex}(a)$ is approximated by the difference of transition energies $\Delta E_{11}(a)-\Delta E_{11}(a=210$ nm). For $a=210$ nm sample, $E_{ex}=1.630$ eV is measured[1] and $E_{11}=1.636$ eV is calculated, thus the heavy-hole exciton binding energy is estimated to be 6 meV. Agreement of our calculations with the experimental data[1] is good.

When a stress Z_z is applied to the QWR, we plot $\Delta E_{ji}(0)$ versus the stress Z_z for the case of $L=1$ nm and $F_y=0$ in Fig. 5. Here we show the transition energies of the ground state of the conduction subband (E^c_1) to the lowest six valence subbands $(E^h_i, i=1-6)$, marked with the indices (j,i). It is interesting to see that anticrossing occurs between all curves. The occurrence of the anticrossing is because of the existence of the off-diagonal elements of the Kohn-Luttinger Hamiltonian (17). For transitions (11) and (12), we observe that (i) $\Delta E_{ji}(0)$ decreases linearly as the tensile stress $Z_z(>0)$ increases and (ii) $\Delta E_{ji}(0)$ increases linearly and then levels off as the compressive stress $Z_z(<0)$ increases because of anticrossing. Curve (12) and curve (13) repel each other; curve (13) and curve (14) repel each other; curve (14) and curve (15) repel each other. When Z_z is compressive (tensile), the transition energies show a blueshift (redshift) because the effective band gap becomes larger (smaller).

When a positive electric field F_y is applied in the y direction of the QWR, the potential profiles tilt and the electrons

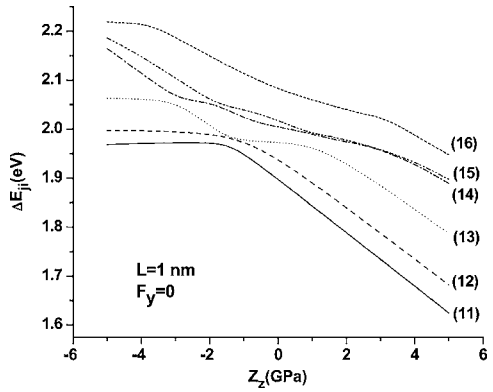

FIG. 5. Optical transition energy versus external stress for the GaAs/AlAs QWR.

move and accumulate near the $y=-a/2$ interface while the holes accumulate near the $y=a/2$ interface. However, if the field strength is too strong, field emission occurs and the electrons or the holes or both are no longer confined and leak out from the QWR to the matrix material. Let this critical field for the field emission to occur be F_{cr}. The optical transition energies $\Delta E_{ji}(0)$ versus the electric field F_y for the case of $L=1$ nm, $Z_z=0$, $j=1$, and $i=1$ to 6 are plotted in Fig. 6. Here, we observe that (i) when $|F_y|$ is less than $F_{\mathrm{cr}}=7$ mV/nm, $\Delta E_{ji}(0)$ increases nearly linearly with F_y and (ii) when $|F_y|$ is larger than $F_{\mathrm{cr}}=7$ mV/nm, the slopes of $d\Delta E_{ji}(0)/dF_y$ show sudden changes which imply the field emission occurs and electrons (not holes) begin to leak out from the QWR. The critical fields for holes are larger because the potential barrier for the holes is higher (see Fig. 1) for the GaAs/AlGaAs QWR. The critical field for a hole in the ground state is about $F_{\mathrm{cr}}=12$ mV/nm.

The oscillator strength $O_{ji}(k_x)$ defined in Eq. (24) is dimensionless and represents the equivalent number of oscillators of the transition for the electron in the jth subband and hole in the ith subband. There are two classes of the momentum matrix element. At the zone center ($k_x=0$), (i) for the dipole-allowed intersubband transitions, the momentum matrix element is greater than zero as depicted in Fig. 7(a) and (ii) for the dipole-forbidden intersubband transitions, the momentum matrix element is zero as depicted in Fig. 7(b) with

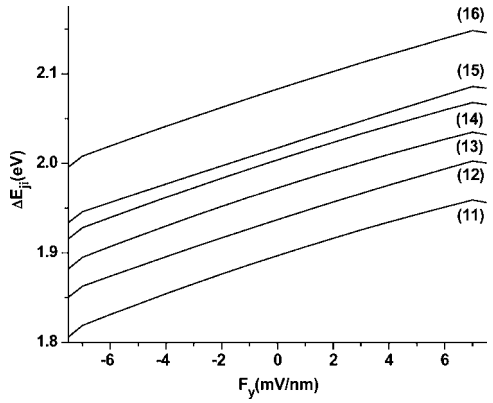

FIG. 6. Optical transition energy versus external electric field for the GaAs/AlAs QWR.

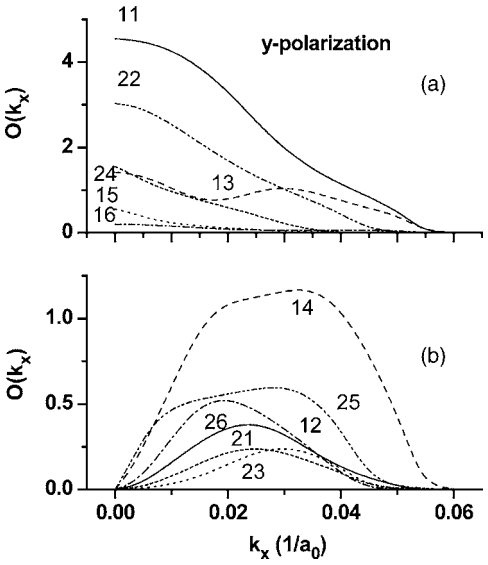

FIG. 7. Oscillator strength as a function of k_x for the (a) dipole-allowed and (b) dipole forbidden intersubband transitions for the GaAs/AlAs QWR.

$L=1$ nm, $Z_z=0$, and $F_y=0$. Here, the polarization is in the y direction and only two (six) of the lowest of conduction (valence) subbands are considered in the calculation. We see that for the allowed transitions O_{11} and O_{22} are stronger, O_{13} and O_{24} are weaker, and O_{15} and O_{16} are negligible. We expect that those optical transitions with stronger oscillator strengths must dominate the optical absorption coefficient.

The joint density of states J_{cv} [Eq. (22)] and the optical absorption coefficient α [Eq. (24)] as a function the optical energy $E_{\mathrm{op}}=\hbar\omega$ are shown in Figs. 8(a)–8(d). The polarization is in the y direction. Figure 8(a) indicates that for

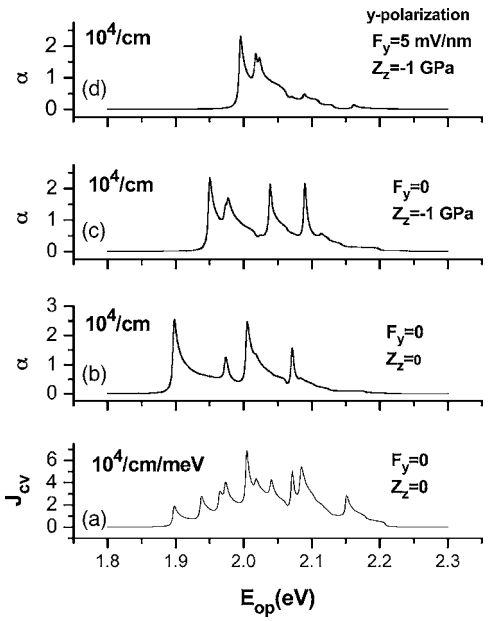

FIG. 8. (a) Joint density of states versus optical energy E_{op}, (b) Optical absorption coefficients α versus E_{op} without fields, and (c) and (d) with various fields for the GaAs/AlAs QWR. Polarization is in the y direction.

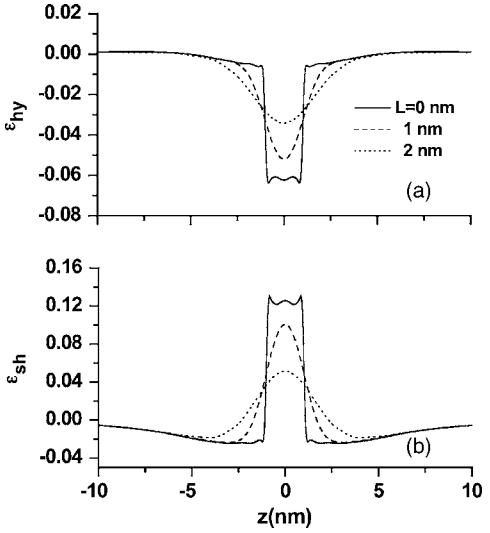

FIG. 9. Strain distributions as a function of z for (a) hydrostatic strain and (b) shear strain, at $y=0$.

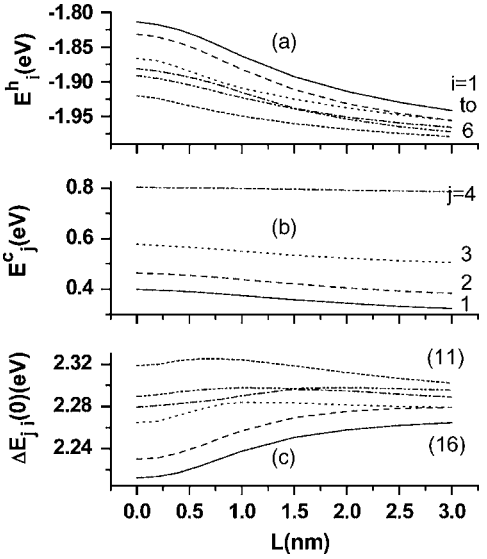

FIG. 10. (a) Valence subbands E^h_i, (b) conduction subbands E^c_j, and (c) ΔE_{ji} at the zone center as a function of the diffusion parameter L without any external fields for the CdSe/ZnSe QWR.

the case of $L=1$ nm, $Z_z=0$, and $F_y=0$, the J_{cv} versus E_{op} shows ten sharp peaks for transitions of Eqs. (11), (12), (21), (13), (22), (15), and (23)–(26). Under the same conditions, Fig. 8(b) plots the optical absorption versus E_{op} and there are four peaks for Eqs. (11), (13), (22), and (24) transitions which agree with the predictions of the oscillator strengths for the allowed transitions mentioned earlier (see Fig. 7). When a compressive stress $Z_z=-1$ GPa is applied to the QWR, the absorption peaks show blueshifts in Fig. 8(c). Further more, when an electric field $F_y=5$ mV/nm is applied, the absorption peaks show even greater blueshifts and the higher energy peaks are diminished. This occurs because the electric field separates the electrons and holes in the QWR region and reduces the oscillator strengths.

B. Strained CdSe/ZnSe QWR

The internal strain due to the lattice mismatch not only shifts the band edges but also deforms the potential profiles of the of the CdSe/ZnSe QWR. When alloy interdiffusion occurs, the abrupt interfaces become gradual and the strain tensor ε_{ij} is reduced from its initial value [Eq. (5)]. Variations of the hydrostatic strain ε_{hy} and shear strain ε_{sh} [Eq. (8)] as a function of z at $y=0$ with the diffusion parameter $L_y=L_z=L$ are plotted in Figs. 9(a) and 9(b), respectively. We observe that both the ε_{hy} and ε_{sh} distributions vary from abrupt to gradual and diminish and become gradual as L increases. The energy band profiles for the CdSe/ZnSe QWR (not shown) look similar to the profiles for the GaAs/AlAs QWR, as shown in Fig. 1 although the cause of the valence band splitting and the effective energy gap widening is different.

The intermixing can influence the energy subbands at the zone center in two ways. When the interdiffusion becomes stronger (i) the internal strain is relaxed and becomes weaker and this leads to the effective band gap shrinkage which increases the barrier heights and (ii) the potential profiles are deformed and the effective band gap may become wider. The interdiffusion effect on the valence subband edges E^h_i $(i=1-6)$ is plotted in Fig. 10(a). Because the barrier height for the holes is much smaller than that for the electrons, the subband shifts due to the deformed potential profile overwhelm the subband shifts due to the internal strain. Thus, when L increases, E^h_i $(i=1-6)$ decreases as shown in Fig. 10(a). Figure 10(b) shows that E^c_j decreases sublinearly as L increases and this result differs from that shown in Fig. 2(b) for the case of the unstrained QWR. This decrease is due to the fact that when the interdiffusion becomes stronger and the internal strain becomes weaker as L becomes larger, the subband shifts due to the internal strain dominate those due to the deformed potential profile. The variation of the optical transition energy $\Delta E_{ji}(0)$ with L is shown in Fig. 10(c) to reflect the combined effects of Figs. 10(a) and 10(b).

The valence subband structures $[E^h_i(k_x),\ i=1,2,3,\ldots,6]$ for the CdSe/ZnSe QWR with $L=1$ nm, $Z_z=0$, $F_y=0$ and with $L=1$ nm, $Z_z=-4$ Gpa, $F_y=0$ are plotted in Figs. 11(a) and 12(b), respectively. In Fig. 12(a), $E^h_i(0)(i=1-6)$ in eV occur at $-1.863\{-\}$, $-1.882\{-\}$, $-1.909\{-\}$, $-1.915\{+\}$, $-1.923\{-\}$, and $-1.950\{+\}$; and in Fig. 12(b), E^h_i (0) in eV are $-1.775\{-\}$, $-1.790\{-\}$, $-1.815\{-\}$, $-1.849\{-\}$, $-1.852\{-\}$, and $-1.853\{-\}$. The curvatures of $E^h_i(0)$ are marked with $\{+\}$ for upward curvature and $\{-\}$ for downward curvature. At the zone center with $Z_z=0(-4$ GPa), we have probability densities $|\Phi^1|^2=0.013(0.281)$, $|\Phi^2|^2=0.948(0.001)$, $|\Phi^3|^2=0.031(0.002)$, and $|\Phi^4|^2=0.008(0.716)$. The dominant component of the hole wave function is similar to what was discussed previously. The variations of $\Delta E_{ji}(0)$ with Z_z, $\Delta E_{ji}(0)$, with F_y and the oscillator strength O_{ji} versus k_x for the dipole transitions are similar to those in unstrained GaAs as shown in Figs. 5–7.

The joint density of states J_{cv} [Eq. (22)] and the optical absorption coefficient α for the y polarization [Eq. (24)] as a function of the optical energy $E_{op}=\hbar\omega$ are shown in Figs. 12(a)–12(d). Figure 12(a) shows that for the case of

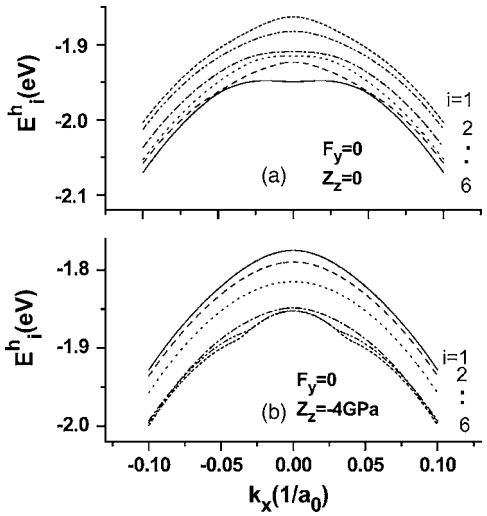

FIG. 11. Valence subband structures for (a) without external fields, and (b) with a stress for the CdSe/ZnSe QWR.

$L=1$ nm, $Z_z=0$, and $F_y=0$, J_{cv} versus E_{op} shows eleven sharp peaks for the transitions (11), (12), (14), (15), (21), (22), (16), and (23)–(26). Note that the transition (13) which is in-between the transitions (12) and (14) is smeared out due to the overlap and does not appear in Fig. 12(a). Figure 12(b) plots the optical absorption α versus E_{op} and there are four peaks located at 2.239 eV (11), 2.286 eV (13), 2.320 eV (22), and 2.363 eV (24) which agree with the oscillator strengths of the y polarization for the allowed transitions. When a compressive stress $Z_z=-2$ is applied to the QWR,

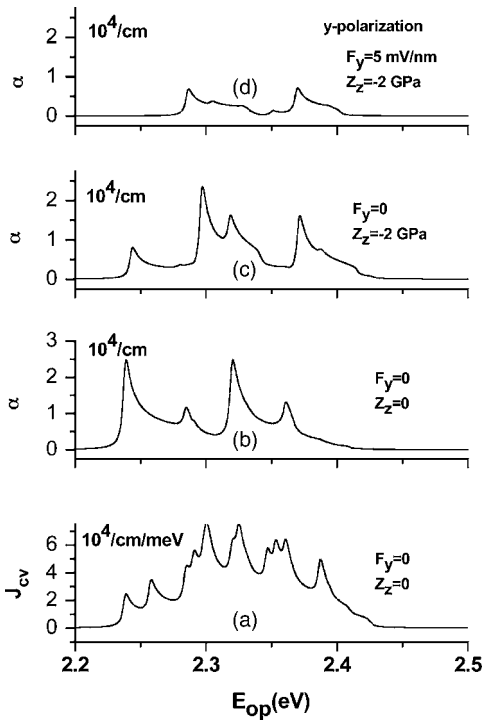

FIG. 12. (a) Joint density of states, (b) optical absorption coefficients α without fields, and (c) and (d) optical absorption coefficients α with various fields versus optical energy E_{op} for the CdSe/ZnSe QWR (y polarization).

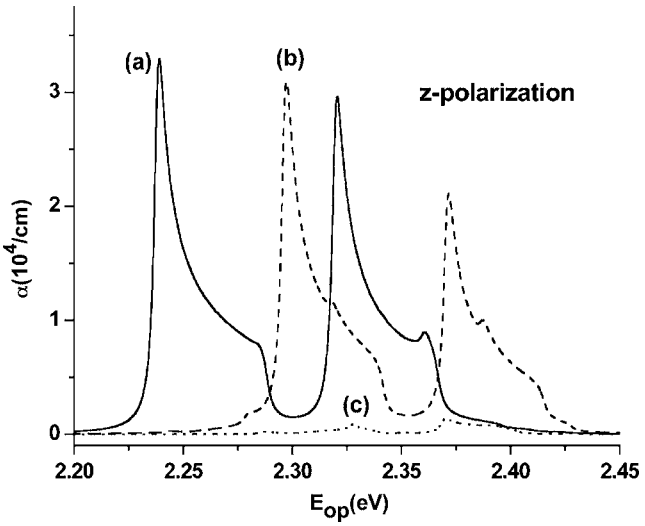

FIG. 13. Optical absorption coefficients α versus E_{op} (a) without fields (b) with Z_z (c) with Z_z and F_y for the CdSe/ZnSe QWR (z polarization).

the absorption peaks show blue shifts in Fig. 12(c). The behavior with electric field shown in Fig. 12(d) is similar to what was discussed previously. The optical absorption coefficients for the z-polarization as a function of the optical energy for $L=1$ nm are shown in Fig. 13 with (a) $F_y=0$, $Z_z=0$, (b) $F_y=0$, $Z_z=-2$ GPa, and (c) $F_y=5$ mV/nm, $Z_z=-2$ GPa. Figure 13(a) shows that there are two major absorption peaks located at 2.239 eV (11), 2.320 eV (22), and a weaker peak at 2.363 eV (25). The behavior of the absorption when the compressive stress Z_z and electric field F_y is applied to the wire is similar to that in GaAs/AlAs wires which was discussed earlier.

IV. CONCLUSIONS

We have studied the optical absorption coefficient of the QWRs in the electric and strain fields with intermixing interfaces. The potential profiles of the conduction and the valence band edges are determined by the intermixing heterojunctions, internal strain due to the lattice mismatch, the external electric field and the external stress. The conduction subband structures for the QWR are described by the single-band Schrödinger equation in the effective mass approximation while the valence subband structures are calculated by using the four-band Kohn-Luttinger Hamiltonian. Some physical properties such as the joint density of states, oscillator strengths and absorption coefficients are formulated in terms of the solutions of the above mentioned matrix equations. We find that the intermixing can influence the optical transition energy $\Delta E_{ji}(0)$. When the interdiffusion becomes stronger, on one hand the internal strain is relaxed leading to the effective band gap shrinkage (if the initial strain $\varepsilon_0<0$), and on the other hand the potential profiles are deformed and the effective band gap becomes wider. Variations of $\Delta E_{ji}(0)$ with external stress show the anticrossing effect between various optical transitions and variations of $\Delta E_{ji}(0)$ with external electric field shows the field emission effect. The os-

cillator strengths of the dipole-allowed intersubband transitions for the y and z polarizations are calculated to infer possible optical transitions in the absorption coefficients. The different polarization of the optical field leads to very different behaviors of the optical absorption coefficients.

ACKNOWLEDGMENTS

The author Wu Ching Chou would like to thank the National Science Council of Taiwan for support under Grant No. NSC93-2112-M-009-031.

[1] P. M. Petroff, A. C. Gossard, R. A. Logan, and W. Wiegmann, Appl. Phys. Lett. **41**, 635 (1982).
[2] F. E. Prins, G. Lehr, M. Burkard, H. Schweizer, M. H. Pilkuhn, and G. W. Smith, Appl. Phys. Lett. **62**, 1365 (1993).
[3] J. M. Gaines, P. M. Petroff, H. Kroemer, R. J. Simes, R. S. Geels, and J. H. English, J. Vac. Sci. Technol. B **6**, 1378 (1988).
[4] E. Kapon, D. M. Hwang, and R. Bhat, Phys. Rev. Lett. **63**, 430 (1989).
[5] P. M. Petroff, M. S. Miller, Y. T. Lu, S. A. Chalmers, H. Metiu, H. Kroemer, and A. C. Gossard, J. Cryst. Growth **111**, 360 (1991).
[6] G. C. Osbourne, Phys. Rev. B **27**, 5126 (1983).
[7] L. D. Nguyen, D. C. Radulescu, M. C. Foisy, P. J. Tasker, and L. F. Eastman, IEEE Trans. Electron Devices **36**, 833 (1989).
[8] P. K. York, K. J. Beernink, G. E. Fernández, and J. J. Coleman, Appl. Phys. Lett. **54**, 499 (1989).
[9] M. Walther, E. Kapon, E. Colas, D. M. Hwang, and R. Bhat, Appl. Phys. Lett. **60**, 52 (1991).
[10] S. Tiwari, G. D. Pettit, K. R. Milkove, F. Legoues, R. J. Davis, and J. M. Woodall, Appl. Phys. Lett. **64**, 3536 (1994).
[11] M. Asada, Y. Miyamoto, and Y. Suematsu, IEEE J. Quantum Electron. **22**, 1915 (1986).
[12] E. Kapon, D. M. Hwang, M. Walther, R. Bhat, and N. G. Stoffel, Surf. Sci. **267**, 593 (1992).
[13] J. C. Yia and N. Dagli, IEEE J. Quantum Electron. **31**, 208 (1995).
[14] D. S. Citrin and Y. Chang, IEEE J. Quantum Electron. **29**, 97 (1993).
[15] M. Notomi, S. Nojima, M. Okamoto, H. Iwamura, T. Tamamura, J. Hammersberg, and H. Weman, Phys. Rev. B **52**, 11 073 (1995).
[16] T. Tadic and Z. Ikoni, Phys. Rev. B **50**, 7680 (1994).
[17] Y. Arakawa, T. Yamauchi, and J. N. Schulman, Phys. Rev. B **43**, 4732 (1991).
[18] G. A. Baraff and D. Gershoni, Phys. Rev. B **43**, 4011 (1991).
[19] O. Stier and D. Bimberg, Phys. Rev. B **55**, 7726 (1997).
[20] M. Grundmann, O. Stier, and D. Bimberg, Phys. Rev. B **50**, 14187 (1994).
[21] L. De Caro and L. Tapfer, J. Appl. Phys. **79**, 9188 (1996).
[22] I. Vurgaftman, J. M. Hinckley, and J. Singh, IEEE J. Quantum Electron. **30**, 75 (1994).
[23] M. Notomi, J. Hammersberg, H. Weman, S. Nojima, H. Sugiura, M. Okamoto, T. Tamamura, and M. Potemski, Phys. Rev. B **52**, 11 147 (1995).
[24] M. Klude, T. Passow, H. Heinke, and D. Hommel, Phys. Status Solidi B **229**, 1029 (2002).
[25] B. Kato, H. Noguchi, M. Nagazi, H. Ohkuyama, S. Kijima, and A. Ishibashi, Electron. Lett. **34**, 282 (1998).
[26] N. Stranski and L. Von Krastanov, Akad. Wiss. Lit. Mainz Abh. Math. Naturwiss. Kl. **146**, 797 (1993).
[27] M. Califano and P. Harrison, J. Appl. Phys. **91**, 389 (2002).
[28] A. D. Andreev, J. R. Downes, D. A. Faux, and E. P. O'Reilly, J. Appl. Phys. **86**, 297 (1999).
[29] J. Cibert and P. M. Petroff, Phys. Rev. B **36**, 3243 (1987).
[30] M. Strassburg, Th. Deniozou, A. Hoffmann, R. Heitz, U. W. Pohl, D. Bimberg, A. Rosenauer, D. Gerthsen, S. Schwedhelm, K. Lischka, and D. Schikora, Appl. Phys. Lett. **76**, 685 (2000).
[31] G. Grosso and G. P. Parravicini, *Solid State Physics* (Academic Press, New York 2000).
[32] N. Samarth, H. Luo, J. K. Furdyna, S. B. Qadri, Y. R. Lee, A. K. Ramdas, and N. Otsuka, Appl. Phys. Lett. **54**, 2680 (1987); T. Dietl, H. Ohno, and F. Matsukura, Phys. Rev. B **63**, 195205 (2001).
[33] T. B. Bahder, Phys. Rev. B **41**, 11 992 (1990).
[34] M. A. Cusack, P. R. Briddon, and M. Jaros, Phys. Rev. B **54**, R2300 (1996).
[35] E. P. Polatilov, V. A. Fonoberov, V. M. Fomin, and J. T. Devreese, Phys. Rev. B **64**, 245328 (2001).
[36] B. A. Foreman, Phys. Rev. B **48**, R4964 (1993).
[37] M. G. Burt, Phys. Rev. B **50**, 7518 (1994).
[38] C. Kittel, *Quantum Theory of Solids* (John Wiley & Sons, New York 1963).
[39] H. C. Casey, Jr. and M. B. Panish, *Heterostructure Lasers* (Academic Press, New York, 1978).
[40] H. J. Lozykowski and V. K. Shastri, J. Appl. Phys. **69**, 3235 (1991).
[41] R. C. Tu, Y. K. Su, D. Y. Lin, C. F. Li, Y. S. Huang, W. H. Lan, S. J. Chang, S. C. Chou, and W. C. Chou, J. Appl. Phys. **83**, 1043 (1998).
[42] D. J. Norris and M. G. Bawendi, Phys. Rev. B **53**, 16 338 (1996).
[43] M. Balkanski and R. F. Wallis, *Semiconductor Physics and Applications* (Oxford University Press, New York, 2000).
[44] N. T. Pelekanos, J. Ding, M. Hagerott, A. V. Numikko, H. Luo, N. Samarth, and J. K. Furdyna, Phys. Rev. B **45**, 6037 (1992).
[45] A. Blacha, H. Presting, and M. Cardona, Phys. Status Solidi B **126**, 11 (1984).
[46] *Semiconductors, Intrinsic Properties of Group IV Elements and III-V, II-VI and I-VII Compounds*, edited by O. Madelung and M. Schulz, Landolt-Börnstein, New Series, Vol. 22, Subvolume a (Spring-Verlag, New York, 1987).
[47] J. I. Pankove, *Optical Processes in Semiconductors* (Dover, New York, 1971).
[48] P. Lawaetz, Phys. Rev. B **4**, 3460 (1971).
[49] I. Vurgaftman, J. R. Meyer, and L. R. Ram-Mohan, J. Appl. Phys. **89**, 5815 (2001).
[50] R. C. Miller, D. A. Kleinman, and A. C. Gossard, Phys. Rev. B **29**, R7085 (1984).